

Rao–Blackwellized Stein Gradient Descent for Joint State–Parameter Estimation

Milad Banitalebi Dehkordi, Manas Mejari, Dario Piga

Abstract—We present a filtering framework for online joint state estimation and parameter identification in nonlinear, time-varying systems. The algorithm uses *Rao–Blackwellization* technique to infer joint state–parameter posteriors efficiently. In particular, conditional state distributions are computed analytically via Kalman filtering, while model parameters—including process and measurement noise covariances—are approximated using particle-based *Stein Variational Gradient Descent* (SVGD), enabling stable real-time inference. We prove a theoretical consistency result by bounding the impact of the SVGD approximated parameter posterior on state estimates, relating the divergence between the true and approximate parameter posteriors to the total variation distance between the resulting state marginals. Performance of the proposed filter is validated on two case studies: a bioreactor with Haldane kinetics and a neural-network-augmented dynamic system. The latter demonstrates the filter’s capacity for online neural network training within a dynamical model, showcasing its potential for fully adaptive, data-driven system identification.

Index Terms—Rao–Blackwellized Filtering, Stein Variational Gradient Descent, joint State–parameter estimation.

I. INTRODUCTION

ACCURATE state estimation requires a well-specified process model and known measurement noise statistics. In practice, however, model parameters and noise covariances are typically unknown and may change over time due to changing operating conditions. Such uncertainties can degrade the performance of the classical filters that assume fixed, known models, leading to substantial state estimation errors from model mismatch [1]. This motivates methods that infer the joint posterior over both states and unknown parameters, enabling improved real-time estimates and principled uncertainty quantification essential for robust control, monitoring, and decision-making [2].

Traditional approaches for joint state and parameter estimation often rely on *augmented* Extended Kalman Filters (EKF), where the parameters are appended to the state vector and updated with the system states. Although augmented EKF have been widely used [3], they are known to perform poorly for highly nonlinear systems. Moreover, learning additional quantities such as process and measurement noise statistics is numerically delicate and may lead to instability or even filter divergence [4]. Several adaptive Kalman filtering methods have been proposed to estimate noise covariances (see, e.g. [5]–[7]), but they typically suffer from sensitivity to model mismatch and tuning issues. Beyond joint estimation settings,

Kalman-based techniques have also been applied to learning problems involving parameter inference alone. For instance, [8] reformulates the training of recurrent neural networks as a state–estimation problem and applies the Extended Kalman Filter (EKF) to obtain second-order–like updates.

Variational Inference (VI) methods can also approximate the joint posterior distribution over states and parameters [9], but they are typically computationally intensive and less suited for real-time applications. Monte Carlo methods, such as Particle Filters (PFs), offer a more flexible framework for approximating complex, potentially non-unimodal distributions [10], [11]. However, a naïve application of PFs to jointly propagate both states and parameters is restrictive for high dimensional systems and often fails to exploit the known structure of the state-space model. Rao–Blackwellized Particle Filters (RBPFs) address this limitation by analytically evaluating the conditional distribution of the states given the parameters and using a Monte Carlo approximation for the parameter distribution [12]–[15]. This approach leverages the prior knowledge encoded in the state-space model while retaining the flexibility of particle-based methods for parameter inference. In standard RBPFs, the temporal evolution of parameters is usually modeled as a stochastic process with additive noise, which is chosen as *proposal distribution* from which the particles are sampled. This introduces an additional hyperparameter, namely the noise covariance for parameter propagation. This often requires careful tuning and can affect the accuracy of both state and parameter estimates.

Recently, Stein Variational Gradient Descent (SVGD) has emerged as a promising deterministic alternative for approximating probability distributions [16]. Unlike PFs, which propagate particles stochastically, weighted based on likelihoods, SVGD evolves particles deterministically along directions that minimize the Kullback–Leibler (KL) divergence between the approximate and true posterior. This makes SVGD appealing in a Rao–Blackwellized framework, where the states can be estimated analytically (e.g., via the EKF) and the parameter distribution is approximated deterministically using SVGD. Building on this, in this paper we introduce the *Rao–Blackwellized Stein Gradient Descent (RBSGD) filter*, where the measurements deterministically steer the particles toward the true parameter distribution. This allows for accurate state estimation, avoiding the need to carefully tune proposal parameters. To the best of our knowledge, the integration of Rao–Blackwellization concepts and SVGD for joint state–parameter estimation has not been proposed before.

In addition, curvature information in the parameter space has been incorporated in variants of SVGD, such as Newton SVGD or L-BFGS SVGD, to improve convergence by

Milad Banitalebi Dehkordi, Manas Mejari, and Dario Piga are with the IDSIA Dalle Molle Institute for Artificial Intelligence, SUPSI-USI, 6962 Lugano, Switzerland (e-mail: {milad.banitalebi, manas.mejari, dario.piga}@supsi.ch). This preprint is submitted to the IEEE Transactions on Automatic Control.

adapting the step size according to the local geometry of the likelihood [17]–[19]. While effective, these approaches typically rely on computing the Hessian of the log-posterior, which introduces significant computational overhead. To address this, in this paper we also propose the *Rao–Blackwellized Fisher Stein Gradient Descent (RBFSGD) filter*, an extension of RBSGD that incorporates the Fisher Information Matrix (FIM) as an indicator of the local parameter space geometry [20]–[22]. The FIM is utilized in two ways: (i) in updating the parameters using a Fisher-adapted Adam scheme, and (ii) in the kernel formulation of SVGD, where the standard Euclidean distance is replaced by a Fisher-informed distance in the RBF kernel. This approach improves the scaling and directionality of parameter updates while maintaining computational tractability.

Finally, we analyze the theoretical properties of the proposed RBSGD and RBFSGD filters. In particular, we establish an upper bound on the ℓ_1 -norm error between the approximate and true marginal state distributions. Furthermore, we prove that under mild assumptions, this bound (i) is related to the KL divergence between the approximate and true parameter posteriors and (ii) monotonically decreases along the SVGD iterations.

The remainder of this paper is organized as follows. In Section II, we formulate the joint estimation problem for states and model parameters. Section III reviews Rao–Blackwellized Particle Filters and their application in state-space models. Building on this foundation, Section IV-A introduces the proposed RBSGD filter, and Section IV-B presents its Fisher-informed extension, the RBFSGD filter. Finally, Section VI demonstrates the performance of the proposed methods on two case studies: a highly nonlinear fed-batch bioreactor and a nonlinear system modelled with neural network.

Notation: Let \mathbb{R}^n denote the set of real vectors with dimension n . The sequence of time-indexed vectors $\{u_1, \dots, u_t\}$ is denoted as $u_{1:t}$ and $z_{t|k}$ denotes the estimate of signal z at time t , given the observations up to and including time k . The Dirac delta function centered at $\bar{\theta}$ is denoted by $\delta_{\bar{\theta}}(\theta)$. A random variable x sampled from a Gaussian distribution with mean μ and covariance Σ is denoted by $x \sim \mathcal{N}(\mu, \Sigma)$. The expected value of a random variable is denoted by $\mathbb{E}[x]$. Given two probability density functions p and q , the KL divergence is denoted as $\text{KL}(p||q)$, which is defined as $\text{KL}(p||q) = \int p(x) \ln \frac{p(x)}{q(x)} dx$.

II. PROBLEM STATEMENT

We consider the following discrete-time nonlinear parameter-varying state–space model,

$$x_{t+1} = f(x_t, u_t, \theta_t) + q_t, \quad (1a)$$

$$y_t = h(x_t, \theta_t) + r_t, \quad (1b)$$

where $t \in \mathbb{N}$ denotes the time index, $x_t \in \mathbb{R}^{n_x}$, $y_t \in \mathbb{R}^{n_y}$, and $u_t \in \mathbb{R}^{n_u}$ denote the system state, output, and input, respectively. The functions f and h describe the nonlinear state transition and measurement mappings and are parameterized by an *unknown* parameter $\theta_t \in \mathbb{R}^{n_\theta}$. The process and measurement noise are modeled as zero-mean Gaussian

random variables, $q_t \sim \mathcal{N}(0, Q(\theta_t))$ and $r_t \sim \mathcal{N}(0, R(\theta_t))$, with corresponding positive definite covariance matrices $Q(\theta_t)$ and $R(\theta_t)$ parameterized by θ_t .

Given the sequence of output measurements $y_{1:t}$ and inputs $u_{1:t}$ up to time t , our objective is to estimate the joint posterior distribution over states and time-varying model parameters $p(x_t, \theta_t | y_{1:t}, u_{1:t})$, at time t . We seek a recursive filter that updates this posterior online, from previous posterior estimate $p(x_{t-1}, \theta_{t-1} | y_{1:t-1}, u_{1:t-1})$. The posterior distribution can be then utilized to compute the point estimates (e.g., maximum a-posteriori (MAP)) of the unknown states x_t , and model parameters θ_t , or to provide marginal state (or parameter) posterior to quantify the uncertainty at each time instance.

We note that in a classical Kalman or Bayesian filtering methods, the dynamic models f and g , as well as covariance matrices Q, R , are typically assumed to be *known*. The performance of the filtering algorithms is thus sensitive to the accuracy of the model and choice of covariances. The estimation of the model as well as covariances is therefore critical for accurate state estimation. In this work, we address this problem by joint estimation of the states x_t and unknown parameters (dynamic model and covariances) encoded via the parameter vector θ_t .

We remark that an exact evaluation of the posterior $p(x_t, \theta_t | u_{1:t}, y_{1:t})$ is computationally intractable, and closed-form solutions exist only in specialized cases, e.g., linear time-invariant dynamics with Gaussian noises. In the following sections, we develop *Rao–Blackwellized Particle Filtering* algorithms that compute an *approximation* of the joint posterior $p(x_t, \theta_t | u_{1:t}, y_{1:t})$ and update it online as new observations become available.

III. RAO–BLACKWELLIZED FILTERING FOR JOINT STATE-PARAMETER ESTIMATION

The posterior $p(x_t, \theta_t | y_{1:t}, u_{1:t})$ can be approximated using Monte Carlo sampling-based methods, which typically consists of generating a sequence of N random samples $\{x_t^{(i)}, \theta_t^{(i)}\}_{i=1}^N$, from a Markov chain, whose stationary distribution is the target posterior $p(x_t, \theta_t | u_{1:t}, y_{1:t})$, which can be then approximated with the following empirical distribution,

$$p(x_t, \theta_t | u_{1:t}, y_{1:t}) \approx \frac{1}{N} \sum_{i=1}^N \delta_{(x_t^{(i)}, \theta_t^{(i)})} (x_t, \theta_t).$$

A potential drawback of this naive implementation is that it requires to draw samples from a high-dimensional joint parameter space (x, θ) , which is computationally restrictive for high dimensions. Instead, in this work, we employ a *Rao–Blackwellization* (RB) approach in which part of the posterior is computed analytically, while only the remaining part is approximated using sampling-based algorithms. The advantage of the RB strategy is that it reduces the size of the space over which the sampling is required.

In particular, in the proposed RB filtering framework, after the joint posterior is factorized as,

$$p(x_t, \theta_t | y_{1:t}, u_{1:t}) = p(x_t | \theta_t, y_{1:t}, u_{1:t}) p(\theta_t | y_{1:t}, u_{1:t}), \quad (2)$$

the conditional distribution $p(x_t | \theta_t, y_{1:t}, u_{1:t})$ is computed analytically via Kalman filtering, while the marginal posterior over the parameters, $p(\theta_t | y_{1:t}, u_{1:t})$, is approximated using variants of particle filters.

Particle filters allow us to treat any type of probability distribution and nonlinearity, without being restricting to linear-Gaussian models. In this setting, we introduce the following two variants of the RB particle filters: *Rao-Blackwellized Stein Gradient Descent* (RBSGD) and *Rao-Blackwellized Fisher Stein Gradient Descent* (RBFSGD) filters.

We first review the standard RB particle filter algorithm, and then build upon this framework to preset RBSGD and RBFSGD filters. For brevity, we drop the dependence of the conditional distributions on inputs $u_{1:t}$ in the rest of the paper.

Rao-Blackwellized Particle Filters

In Rao-Blackwellized Particle Filters (RBPFS), [12] a weighted set of N particles $\{w_t^{(i)}, \theta_t^{(i)}\}_{i=1}^N$, *i.e.*, samples from a *proposal distribution* $q(\cdot)$ and their weights, are used to approximate the parameter posterior $p(\theta_t | y_{1:t})$ in (2) by the empirical point-mass distribution as follows,

$$p(\theta_t | y_{1:t}) \approx \sum_{i=1}^N w_t^{(i)} \delta_{\theta_t^{(i)}}(\theta_t), \quad \sum_{i=1}^N w_t^{(i)} = 1, \quad (3)$$

and for each particle $\theta^{(i)}$ (representing the i -th model), an *Extended Kalman Filter* (EKF) is employed to compute the corresponding conditional state distribution $p(x_t^{(i)} | \theta_t^{(i)}, y_{1:t})$. Note that marginalizing out the state variable allows analytic computation of state posterior, $p(x_t^{(i)} | \theta_t^{(i)}, y_{1:t})$ which is the Gaussian posterior distribution derived from EKF given as,

$$p(x_t^{(i)} | \theta_t^{(i)}, y_{1:t}) = \mathcal{N}(x_t^{(i)}; \hat{x}_{t|t}^{(i)}, P_{t|t}^{(i)}), \quad (4)$$

where $\hat{x}_{t|t}^{(i)}, P_{t|t}^{(i)}$ denote the mean and covariance of the state associated with the i -th particle respectively.

RBPFS proceed in three stages: prediction, update, and resampling, as summarized in Algorithm 1. At the initial Step 1, the particles and their weights as well as Kalman filter's mean and covariances are initialized according to prior distributions and initial values.

In the prediction Step 2-3, both state and parameter distributions are propagated forward in time. The parameters evolve according to the following stationary stochastic transition model with additive Gaussian noise,

$$\theta_t^{(i)} = \theta_{t-1}^{(i)} + \eta_t^{(i)}, \quad \eta_t^{(i)} \sim \mathcal{N}(0, \Sigma_\theta), \quad (5)$$

where Σ_θ controls the degree of parameter drift, allowing adaptation to time-varying dynamics. In common practice, the parameter proposal distribution $q(\theta_t | \theta_{t-1}^{(i)})$ is taken as the transition model $p(\theta_t | \theta_{t-1}^{(i)})$. Thus, the proposal $q(\theta_t | \theta_{t-1}^{(i)})$ is Gaussian, with mean $\theta_{t-1}^{(i)}$ and covariance Σ_θ . For each particle $\theta_t^{(i)}$, an EKF is run for state estimation. The state prediction in the EKF follows the system dynamics by linearizing the model (1) as follows,

$$\hat{x}_{t|t-1}^{(i)} = f(\hat{x}_{t-1|t-1}^{(i)}, u_{t-1}, \theta_{t-1}^{(i)}), \quad (6a)$$

$$P_{t|t-1}^{(i)} = F_{t-1}^{(i)} P_{t-1|t-1}^{(i)} (F_{t-1}^{(i)})^\top + Q(\theta_{t-1}^{(i)}), \quad (6b)$$

where $\hat{x}_{t|t-1}^{(i)}$ and $\hat{x}_{t-1|t-1}^{(i)}$ denote the predicted and previous state means, $P_{t|t-1}^{(i)}, P_{t-1|t-1}^{(i)}$ are the corresponding state covariance matrices, and $F_{t-1}^{(i)} = \frac{\partial f}{\partial x}$ is the Jacobian of the dynamics f , evaluated at $\hat{x}_{t-1|t-1}^{(i)}$ and $\theta_{t-1}^{(i)}$.

Upon receiving the observation y_t , the Kalman gain for each particle is computed as

$$K_t^{(i)} = P_{t|t-1}^{(i)} (H_t^{(i)})^\top (H_t^{(i)} P_{t|t-1}^{(i)} (H_t^{(i)})^\top + R(\theta_{t-1}^{(i)}))^{-1}, \quad (7)$$

where Jacobian $H_t^{(i)} = \frac{\partial h}{\partial x}$ of the measurement model g is evaluated at $\hat{x}_{t|t-1}^{(i)}$ and $\theta_{t-1}^{(i)}$, and the innovation covariance is defined as

$$S_t^{(i)} = H_t^{(i)} P_{t|t-1}^{(i)} (H_t^{(i)})^\top + R(\theta_{t-1}^{(i)}). \quad (8)$$

Next, in the update Step 5, the mean and covariance update of the state $x_t^{(i)}$, which form the Gaussian posterior (4) are computed as,

$$\hat{x}_{t|t}^{(i)} = \hat{x}_{t|t-1}^{(i)} + K_t^{(i)} (y_t - h(\hat{x}_{t|t-1}^{(i)}, \theta_{t-1}^{(i)})), \quad (9a)$$

$$P_{t|t}^{(i)} = (I - K_t^{(i)} H_t^{(i)}) P_{t|t-1}^{(i)}. \quad (9b)$$

In the particle weight update Step 4, the importance weights are updated according to the likelihood of the new measurement as ¹,

$$w_t^{(i)} \propto w_{t-1}^{(i)} p(y_t | \theta_{1:t}^{(i)}, y_{1:t-1}) \frac{p(\theta_t^{(i)} | \theta_{t-1}^{(i)})}{q(\theta_t^{(i)} | \theta_{t-1}^{(i)})}, \quad (10a)$$

$$p(y_t | \theta_{1:t}^{(i)}, y_{1:t-1}) = \mathcal{N}(y_t; h(\hat{x}_{t|t-1}^{(i)}, \theta_t^{(i)}), S_t^{(i)}). \quad (10b)$$

To prevent particle degeneracy, *resampling* Step 6 is performed when the effective sample size (ESS) falls below a given threshold n_{thr} . Particles with higher weights are replicated by sampling from a new probability distribution $\theta \sim \sum_{j=1}^N w_t^{(j)} \delta_{\theta_t^{(j)}}(\theta)$, while those with negligible weights are discarded, and all resampled particles are assigned uniform weights, $w_t^{(i)} = 1/N$, preserving a consistent particle population.

In summary, the RBPF Algorithm 1 produces at each time step t a set of weighted samples $\{w_t^{(i)}, \theta_t^{(i)}, \hat{x}_{t|t}^{(i)}, P_{t|t}^{(i)}\}_{i=1}^N$. Then, from (3) and (4), the joint posterior in (2) is approximated with RBPF as,

$$p(x_t, \theta_t | y_{1:t}) \approx \sum_{i=1}^N w_t^{(i)} \delta_{\theta_t^{(i)}}(\theta_t) \mathcal{N}(x_t; \hat{x}_{t|t}^{(i)}, P_{t|t}^{(i)}). \quad (11)$$

IV. RAO-BLACKWELLIZED FILTERING WITH STEIN GRADIENT DESCENT

The RBPF framework discussed in the previous section combines analytical filtering for state estimation with a particle filters approximation for parameter inference, achieving a balance between computational tractability and flexibility in representing non-Gaussian parameter distributions.

However, the performance of the algorithm critically depends on choosing an appropriate proposal distribution

¹In the derivation of RBPF, we typically work on the full trajectory posterior $p(x_{0:t}, \theta_{0:t} | y_{1:t})$ and then marginalize to get $p(x_t, \theta_t | y_{1:t})$.

Algorithm 1 Rao–Blackwellized Particle Filter

Require: Number of particles N , priors for initial parameter and state: $p(\theta_0), p(x_0)$; initial state covariance \bar{P}_0 ; proposal distribution $q(\theta_t | \theta_{t-1})$, resampling threshold n_{thr} .

1: Initialization:
for $i = 1$ to N

 Sample $\theta_0^{(i)} \sim p(\theta_0)$

 Set $\hat{x}_0^{(i)} \sim p(x_0), P_0^{(i)} = \bar{P}_0$ ▷ Initial KF state
 $w_0^{(i)} \leftarrow 1/N$
end for
for $t = 1$ to T
for $i = 1$ to N
2: Particle prediction: $\theta_t^{(i)} \sim q(\theta_t | \theta_{t-1}^{(i)})$ (5)

3: Kalman prediction: Compute $\hat{x}_{t|t-1}^{(i)}, P_{t|t-1}^{(i)}$ (6)

4: Weight update: $\tilde{w}_t^{(i)}$ as in (10a)

5: Kalman update: Compute $\hat{x}_t^{(i)}, P_t^{(i)}$: eq. (9)

end for

 Normalize $w_t^{(i)} = \tilde{w}_t^{(i)} / \sum_{j=1}^N \tilde{w}_t^{(j)}$, $i = 1, \dots, N$.

6: Resample particles according to the weight $w_t^{(i)}$ if $\text{ESS} = 1 / \sum_{i=1}^N (w_t^{(i)})^2 < n_{\text{thr}}$
for $i = 1$ to N

 resample $\theta_t^{(i)}$ from the pdf $\sum_{j=1}^N w_t^{(j)} \delta_{\theta_t^{(j)}}(\theta_t^{(i)})$

 set $w_t^{(i)} \leftarrow 1/N$
end for
end for
return $\{\{\hat{x}_{t|t}^{(i)}, P_{t|t}^{(i)}, \theta_t^{(i)}\}_{i=1}^N\}_{t=1}^T$

$q(\theta_t | \theta_{t-1})$, which can be chosen based on the stochastic transition model (5) for the parameters. This, in turn, requires careful tuning of the noise covariance Σ_θ , to reflect the temporal variability in the parameters. A high-variance proposal spreads particles into low-probability regions, causing weight degeneracy, while a low-variance proposal restricts exploration and yields an overly concentrated and inaccurate posterior approximation. Determining the optimal proposal parameters for a specific target posterior distribution is therefore nontrivial in particle filtering. In addition, accurate approximation of the parameter posterior (3) may require a large number of particles, which can lead to significant computational overhead.

To address these challenges, we adopt a *deterministic Stein Variational Gradient Descent* (SVGD) [16] framework, where particles evolve via a gradient-based update that minimizes the Kullback–Leibler (KL) divergence between the true posterior and its particle approximation. This automatically balances particle exploration and concentration in high-posterior-density regions, eliminating the need to tune the variance parameter Σ_θ to trade off these effects. In the next sections, we introduce two variants of RBPFs where the SVGD method [16] is employed to govern the particle evolution and approximation of the parameter posterior $p(\theta_t | y_{1:t})$ within a Rao–Blackwellization framework, offering an efficient alternatives to the classical RBPFs.

A. Rao–Blackwellized Stein Gradient Descent Filter

In this section, we discuss how to integrate SVGD into the Rao–Blackwellization framework with a Kalman filter for joint state-parameter posterior computation.

The SVGD [16] is a deterministic, particle-based variational inference method for approximating posterior distributions. In SVGD, instead of a stochastic transition model as in (5), the particles $\theta_t^{(i)}$ evolve via a specific *transport map*, i.e., a small perturbation of the identity map: $\theta + \epsilon \phi(\theta)$, where ϵ is a small constant and ϕ is a smooth function. This transformation iteratively transport proposal distribution $\theta \sim q(\theta) = \sum_{i=1}^N \delta_{\theta^{(i)}}(\theta)$ of the particles toward the target posterior $p(\theta | y_{1:t})$. Specifically, SVGD considers the following transformation of the particles:

$$T_{\epsilon\phi} : \theta^{(i)} \mapsto \theta^{(i)} + \epsilon \phi_{q,p}^*(\theta^{(i)}), \quad (12)$$

where $\epsilon > 0$ is a step size representing perturbation magnitude and $\phi_{q,p}^*(\cdot) \in \mathcal{H}$ is the optimal perturbation direction that lies in a vector-valued Reproducing Kernel Hilbert Space \mathcal{H} (RKHS²) with associated positive definite kernel $k(\theta, \theta')$. We next explain the intuition behind $\phi_{q,p}^*(\cdot)$ and show that it maximally decreases the KL divergence between the proposal q and target posterior p . The optimal perturbation direction $\phi_{q,p}^*(\theta)$ in (12) (which depends on both proposal and target distributions q, p as emphasized in the subscript), is given by the following expectation [16],

$$\phi_{q,p}^*(\theta) = \mathbb{E}_{\theta' \sim q(\theta)} \left[k(\theta', \theta) \nabla_{\theta'} \log p(\theta' | y_{1:t}) + \nabla_{\theta'} k(\theta', \theta) \right], \quad (13)$$

where $k(\theta, \theta')$ is a user-defined positive-definite kernel, e.g., the radial basis function $k(\theta, \theta') = \exp(-\frac{1}{h} \|\theta - \theta'\|^2)$, and $\nabla_{\theta'} \log p(\theta' | y_{1:t})$ is the gradient of the log-posterior evaluated at θ' . In (13), the first term drives the particles toward regions of high posterior probability, while the second term introduces repulsion to maintain particle spread, preventing all particle to collapse into local modes of the posterior. This automatically balances particle exploration with concentration in high-density areas.

It can be proved that $\phi_{q,p}^*$ in (13) is the optimal perturbation direction that gives the steepest descent on the KL divergence between proposal and target posterior. The result is formally stated in the following lemma from [16].

Lemma 1. *Consider the transformation in (12): $T_{\epsilon\phi}(\theta) = \theta + \epsilon\phi(\theta)$ and transformed particles $z = T_{\epsilon\phi}(\theta)$ with $\theta \sim q(\theta)$. Let $q_{[T_{\epsilon\phi}]}(z)$ denote the probability density of the particles after this transformation³. Then at the population limit ($N \rightarrow \infty$), the perturbation direction $\phi_{q,p}^*$ in (13) is,*

$$\phi_{q,p}^* = \arg \max_{\phi \in \mathcal{H}, \|\phi\|_{\mathcal{H}} \leq 1} \left\{ -\nabla_{\epsilon} \text{KL}(q_{[T_{\epsilon\phi}]} \| p) \Big|_{\epsilon=0} \right\}, \quad (14)$$

i.e., $\phi_{q,p}^*$ is the direction of the steepest descent that maximizes the negative gradient of the KL term.

²The RKHS of a positive definite kernel $k(x, x')$ is the closure of the linear span $\{f : f(x) = \sum_{i=1}^m a_i k(x, x_i), a_i \in \mathbb{R}\}$, equipped with inner products $\langle f, g \rangle_{\mathcal{H}} = \sum_{i,j} a_i b_j k(x_i, x_j)$ for $g(x) = \sum_i b_i k(x, x_i)$.

³The density for $z = T(\theta)$ is $q_{[T]}(z) = q(T^{-1}(z)) \cdot |\det((\nabla_z T^{-1}(z))|$.

We refer the reader to [16, Theorem 3.1, Lemma 3.2] for details and proofs.

Lemma 1 states that the optimal perturbation direction $\hat{\phi}_{q,p}^*$ maximally decreases the KL divergence between the transformed proposal q after the infinitesimal transformation of the particles $\theta \mapsto \theta + \epsilon \hat{\phi}(\theta)$ and the target posterior p . This result allows for an *iterative* procedure that transforms initial proposal $q_0(\theta)$ towards the target $p(\theta)$: starting from applying the transform $T_0(\theta) = \theta + \epsilon \hat{\phi}_{q_0,p}^*$ on q_0 decreases the KL divergence. This would give a new distribution q_1 , on which again applying the transformation $T_1(\theta) = \theta + \epsilon \hat{\phi}_{q_1,p}^*$ would further decrease the KL divergence. Repeating this process results in a sequence of distributions $\{q_m\}_{m=1}^M$ between q_0 and p via $T_m(\theta) = \theta + \epsilon \hat{\phi}_{q_m,p}^*(\theta)$ for $m = 1, \dots, M$. The following proposition establishes that, under standard smoothness assumptions, each SVGD step decreases the KL divergence to the target posterior for sufficiently small step sizes.

Proposition 1. *Assume that target distribution $\pi_t(\theta) = p(\theta_t|y_{1:t})$ at time t is twice continuously differentiable with bounded Hessian and that the SVGD kernel $k(\theta_t, \theta'_t)$ is bounded and smooth. Consider a sequence of proposal distributions $\{q_{t,m}\}_{m \geq 0}$ where $q_{t,m}$ denotes the proposal distribution at time t for the m -th iteration. Then at the population limit ($N \rightarrow \infty$), when $q_{t,m-1} \neq \pi_t$, there exists $\epsilon_0 > 0$, such that for all step sizes $\epsilon : 0 < \epsilon < \epsilon_0$,*

$$\text{KL}(q_{t,m} \parallel \pi_t) < \text{KL}(q_{t,m-1} \parallel \pi_t). \quad (15)$$

We refer to Appendix A for the proof of Proposition 1.

The result in Proposition 1 allows to formulate the following iterative update of the particles at time t ,

$$\theta_{t,m}^{(i)} = \theta_{t,m-1}^{(i)} + \epsilon \hat{\phi}^*(\theta_{t,m-1}^{(i)}), \quad (16)$$

where $\theta_{t,m}^{(i)}$ denotes the i -th particle at iteration m , at time t and $\hat{\phi}^*(\cdot)$ is an *empirical approximation* of the perturbation direction in (13), computed based on averages taken over N particles as follows,

$$\hat{\phi}^*(\theta) = \frac{1}{N} \sum_{j=1}^N [k(\theta_{t,m}^{(j)}, \theta) \nabla_{\theta_{t,m}^{(j)}} \log p(\theta_{t,m}^{(j)}|y_{1:t}) + \nabla_{\theta_{t,m}^{(j)}} k(\theta_{t,m}^{(j)}, \theta)]. \quad (17)$$

Note that the target posterior is unknown due to its intractable normalization constant, however, as the gradient of the log-posterior is unaffected by additive constants, $\nabla_{\theta_{t,m}^{(j)}} \log p(\theta_{t,m}^{(j)}|y_{1:t})$ in (17) can be computed directly from the unnormalized posterior as follows⁴,

$$\nabla_{\theta} \log p(\theta|y_{1:t}) = \nabla_{\theta} \log p(y_t|\theta, y_{1:t-1}) + \nabla_{\theta} \log p(\theta|y_{1:t-1}),$$

where the first term $p(y_t|\theta, y_{1:t-1})$ is the marginal likelihood computed from the Kalman filter iterations as in (10b), and the second term is the gradient of the log-posterior computed at the previous time step $t-1$. Thus, at the next SVGD iteration

m , the particles are updated via the empirical version of the deterministic transformation $T_m(\theta_{t,m}^{(i)}) := \theta_{t,m-1}^{(i)} + \epsilon \hat{\phi}^*(\theta_{t,m-1}^{(i)})$ as in (16) with perturbation direction as in (17).

We now integrate the SVGD in our Rao-Blackwellization framework to approximate the joint posterior $p(x_t, \theta_t|y_{1:t})$. The iterative algorithm is referred to as *Rao-Blackwellized Stein Gradient Descent* (RBSGD). The RBSGD procedure at time step t is summarized in Algorithm 2. In the RBSGD Algorithm 2, at each time step, the conditional state mean and covariance are first updated via the EKF, followed by a deterministic SVGD update of the parameter particles for M iterations. In particular, in the Kalman prediction and update steps state mean and covariance $\hat{x}_{t|t}, P_{t|t}$ are computed. Next, starting from the particle initialization $\theta_{t-1}^{(i)}$ obtained at $t-1$, the particles $\{\theta_t^{(i)}\}_{i=1}^N$ are iteratively updated according to the SVGD transformation (16) for M iterations, where the perturbation direction $\hat{\phi}^*$ depends on the gradient of the log-likelihood of the Kalman filter as in (10b) and a user-chosen kernel function $k(\theta, \theta')$. For each particle, the conditional state distribution $p(x_t^{(i)}|\theta_t^{(i)}, y_{1:t})$ is computed analytically as in (4) using an EKF. Consequently, the RBSGD maintains the Rao-Blackwellized decomposition, but replaces the stochastic propagation of parameters with a deterministic SVGD-based update, thereby eliminating the need for manual tuning of Σ_{θ} in (5). The resulting algorithm combines the analytical efficiency of Kalman filtering with the deterministic convergence properties of SVGD, offering improved sample efficiency and stability in tracking time-varying parameters.

Algorithm 2 Rao-Blackwellized Stein Gradient Descent Filter

Require: Measurement y_t , State mean and covariance $\{\hat{x}_{t-1|t-1}, P_{t-1|t-1}\}_{i=1}^N$, previous particles $\{\theta_{t-1}^{(i)}\}_{i=1}^N$, RBF kernel $k(\theta, \theta')$, SVGD step size $\epsilon > 0$

for $i = 1$ to N **do**

Kalman Prediction: $\hat{x}_{t|t-1}, P_{t|t-1}$ using (6)

Kalman Update: $\hat{x}_{t|t}, P_{t|t}$ using (9)

Particle Update:

$\theta_{t,0}^{(i)} \leftarrow \theta_{t-1}^{(i)}, i = 1, \dots, N$

for $m = 1$ to M **do**

$\theta_{t,m}^{(i)} \leftarrow \theta_{t,m-1}^{(i)} + \epsilon \hat{\phi}^*(\theta_{t,m-1}^{(i)})$ using (16)-(17) ⁵

end for

$\theta_t^{(i)} \leftarrow \theta_{t,M}^{(i)}$

end for

return $\{\hat{x}_{t|t}, P_{t|t}, \theta_t^{(i)}\}_{i=1}^N$

B. Rao-Blackwellized Fisher Stein Gradient Descent Filter

While the RBSGD filter mitigates particle degeneracy and enhances stability by eliminating the dependence on the proposals with deterministic SVGD updates, its *first-order* optimization dynamics (16) may be slow or poorly conditioned when the posterior exhibits strong curvature or parameter correlations. To address this, we introduce the *Rao-Blackwellized*

⁵Parameter update can be optionally done with an adaptive step size ϵ provided by the Adam algorithm.

⁴dropping the time and iteration index t, m for brevity

Fisher Stein Gradient Descent (RBFSGD) filter, which incorporates *second-order* information via the *Fisher Information Matrix (FIM)*. Similar to natural-gradient and Fisher-based optimization methods [20], [21], RBFSGD uses the FIM as a positive semi-definite curvature approximation of the log-likelihood, preconditioning gradient directions to achieve better-conditioned, directionally informed updates without the computational cost of full Hessian evaluation [23]–[25].

In FSGD, the SVGD particle update in (16) is modified by incorporating second-order information as follows [21],

$$\theta_{t,m}^{(i)} = \theta_{t,m-1}^{(i)} + \epsilon \mathcal{F}(\theta_{t,m-1}^{(i)}) \hat{\phi}^*(\theta_{t,m-1}^{(i)}) \quad (18)$$

where $\mathcal{F}(\theta) \in \mathbb{R}^{n_\theta \times n_\theta}$ is the symmetric positive semi-definite FIM with respect to the parameters θ , defined based on the marginal likelihood as follows,

$$\mathcal{F}(\theta) = \mathbb{E}_{y_t \sim p(y_t | \theta, y_{1:t-1})} \left[\nabla_\theta \log p(y_t | \theta, y_{1:t-1}) \times (\nabla_\theta \log p(y_t | \theta, y_{1:t-1}))^\top \right], \quad (19)$$

In practice, the expectation in (19) is generally intractable, thus it is approximated empirically using the available particles $\theta^{(i)}$ as,

$$\hat{\mathcal{F}}_{\text{lik}} = \frac{1}{N} \sum_{i=1}^N \nabla_{\theta^{(i)}} \log p(y_t | \theta^{(i)}, y_{1:t-1}; \hat{x}_{t|t-1}^{(i)}, S_t^{(i)}) \times (\nabla_{\theta^{(i)}} \log p(y_t | \theta^{(i)}, y_{1:t-1}; \hat{x}_{t|t-1}^{(i)}, S_t^{(i)}))^\top. \quad (20)$$

where $\hat{\mathcal{F}}_{\text{lik}}$ captures the local curvature of the Gaussian log-likelihood of the Kalman filter in (10b) with respect to the parameters. Further, the empirical FIM in (20) is employed to construct the *Fisher-informed* RBF kernel $k_{\mathcal{F}}(\theta, \theta')$ as follows,

$$k_{\mathcal{F}}(\theta^{(i)}, \theta^{(j)}) = \exp\left(-\frac{1}{h} (\theta^{(i)} - \theta^{(j)})^\top \hat{\mathcal{F}}_{\text{lik}} (\theta^{(i)} - \theta^{(j)})\right), \quad (21)$$

which, in turn, is employed in the computation of the perturbation direction $\hat{\phi}^*(\theta)$ in the FSGD update (18). With respect to the RBF kernel $k(\theta, \theta')$ used in SVGD, the Fisher-informed kernel $k_{\mathcal{F}}(\theta^{(i)}, \theta^{(j)})$ in (21) accounts for the anisotropic parameter sensitivities by adapting the similarity metric between particles according to local curvature.

Similar to \mathcal{F}_{lik} in (20), an empirical FIM can be defined using the SVGD perturbation direction as follows,

$$\hat{\mathcal{F}}_{\text{svgd}} = \frac{1}{N} \sum_{i=1}^N \hat{\phi}^*(\theta^{(i)}) \hat{\phi}^*(\theta^{(i)})^\top, \quad (22)$$

where $\hat{\phi}^*(\theta^{(i)})$ is the update direction expressed as in (17), replacing the RBF with the Fisher-informed RBF given in (21).

We now present FSGD algorithm for parameter updates incorporating Fisher information matrices (20)–(22). The parameter particles are updated using a Fisher-preconditioned variant of the Adam optimizer, known as Fisher–Adam [21]. The iterative update for particle $\theta^{(i)}$ at the m -th iteration at time t is given by,

$$\theta_{t,m}^{(i)} = \theta_{t,m-1}^{(i)} + \epsilon (l_{t,m}^{(i)})^{-1} \hat{g}_{t,m}^{(i)}, \quad (23)$$

where ϵ is the step size, and the auxiliary variables $l_{t,m}, \hat{g}_{t,m}$ evolve according to the following update rules:

$$g_{t,m}^{(i)} = \beta_1 g_{t,m-1}^{(i)} + (1 - \beta_1) \hat{\phi}^*(\theta_{t,m-1}^{(i)}), \quad (24a)$$

$$v_{t,m}^{(i)} = \beta_2 v_{t,m-1}^{(i)} + (1 - \beta_2) \hat{\mathcal{F}}_{\text{svgd}}, \quad (24b)$$

$$\hat{g}_{t,m}^{(i)} = \frac{g_{t,m}^{(i)}}{1 - \beta_1^m}, \quad (24c)$$

$$\hat{v}_{t,m}^{(i)} = \frac{v_m^{(i)}}{1 - \beta_2^m}, \quad (24d)$$

$$l_{t,m}^{(i)} l_{t,m}^{(i)\top} = \hat{v}_{t,m}^{(i)}. \quad (24e)$$

Here, $g_{t,m}^{(i)}$ and $v_{t,m}^{(i)}$ denote the first and second moment estimates of the parameter $\theta_{t,m}^{(i)}$, respectively, and $\hat{g}_m^{(i)}$ and $\hat{v}_m^{(i)}$ are their bias-corrected counterparts. The term $l_{t,m}^{(i)}$ is the Cholesky factor of $\hat{v}_{t,m}^{(i)}$. The parameters β_1 and β_2 are exponential decay rates (typically set to $\beta_1 = 0.9$ and $\beta_2 = 0.999$), $\hat{\phi}^*(\theta^{(i)})$ is the FSGD update direction as in (17) with fisher-informed kernel in (21), and $\hat{\mathcal{F}}_{\text{svgd}}$ is the empirical FIM computed as in (22). This formulation allows the parameter updates to incorporate local curvature information efficiently, improving convergence and stability compared to standard first-order SVGD updates (16).

As in RBSGD, we integrate the FSGD particle update (23) in the Rao-Blackwellized framework. The resulting RBFSGD procedure at time t is summarized in Algorithm 3. At each time step t , the conditional state mean $\hat{x}_{t|t}$ and covariance $P_{t|t}$ are first updated via the Kalman filter, followed by calculation of the FIMs (20)–(22). Finally, the parameters are updated by taking M Fisher–Adam steps as in (23).

Algorithm 3 Rao–Blackwellized Fisher Stein Gradient Descent Filter

Require: Measurement y_t , EKF mean state and covariance $\{\hat{x}_{t-1|t-1}, P_{t-1|t-1}\}_{i=1}^N$, particles $\{\theta_{t-1}^{(i)}\}_{i=1}^N$, Fisher informed kernel $k_{\mathcal{F}}(\cdot, \cdot)$, step size ϵ

for $i = 1$ to N **do**

Kalman Predict $\hat{x}_{t|t-1}, P_{t|t-1}$ via (6)

Kalman Update $\hat{x}_{t|t}, P_{t|t}$ via (9)

end for

Compute $\hat{\mathcal{F}}_{\text{lik}}$ and $\hat{\mathcal{F}}_{\text{svgd}}$ using (20) and (22)

Particle Update:

$\theta_{t,0}^{(i)} \leftarrow \theta_{t-1}^{(i)}, i = 1, \dots, N$

for $i = 1$ to N **do**

for $m = 1$ to M **do**

Update $\theta_{t,m}^{(i)}$ using Fisher–Adam step (23)

end for

$\theta_t^{(i)} \leftarrow \theta_{t,M}^{(i)}$

end for

return $\{\hat{x}_{t|t}, P_{t|t}, \theta_t^{(i)}\}_{i=1}^N$

V. THEORETICAL BOUNDS ON POSTERIOR APPROXIMATION ERROR

Once the joint posterior is approximated with RBSGD or RBFSGD algorithms, we can compute the marginal state posterior. In this section, we derive bounds on the approximation

error in the marginal state posterior due to the approximate parameter posterior.

As in the RBPf (11), we can obtain an approximation of the joint posterior with RBSGD and RBFSGD filters as,

$$\tilde{p}(x_t, \theta_t | y_{1:t}) = \frac{1}{N} \sum_{i=1}^N \delta_{\theta_t^{(i)}}(\theta_t) \mathcal{N}(x_t; \hat{x}_{t|t}^{(i)}, P_{t|t}^{(i)}), \quad (25)$$

where $\{\theta_t^{(i)}\}_{i=1}^N$ are the particles (with equal weights $\frac{1}{N}$) deterministically transported towards the target posterior $p(\theta_t | y_{1:t})$.

From (25) we can compute the *marginal* state posterior approximation by integrating out the particles,

$$\tilde{p}(x_t | y_{1:t}) = \sum_{i=1}^N \tilde{p}(x_t, \theta_t^{(i)} | y_{1:t}) = \frac{1}{N} \sum_{i=1}^N \mathcal{N}(x_t; \hat{x}_{t|t}^{(i)}, P_{t|t}^{(i)}), \quad (26)$$

as $\delta_{\theta_t^{(i)}}(\theta^{(i)}) = 1$ and 0 otherwise.

Remark 1. The representation in (26) highlights a key advantage of the RBSGD/RBFSGD framework: the marginal approximated state posterior is a *Gaussian mixture*, in contrast to *augmented EKF* approaches, which impose a *Gaussian* approximation on the joint state–parameter vector and thus force the marginal state posterior to remain Gaussian. The mixture form in (26) naturally captures multi-modality, skewness, and other nonlinear effects induced by parameter uncertainty, resulting in a more expressive and often more accurate posterior representation.

Remark 2 (MAP estimates). The joint posterior can also be used to compute the *maximum a-posteriori* (MAP) estimates $x_t^{\text{MAP}}, \theta_t^{\text{MAP}}$ as,

$$\begin{aligned} x_{\text{MAP}}, \theta_{\text{MAP}} &= \arg \max_{x_t, \theta_t} \tilde{p}(x_t, \theta_t | y_{1:t}) \\ &= \arg \max_{x_t, \{\theta_t^{(i)}\}_{i=1}^N} \mathcal{N}(x_t; \hat{x}_{t|t}^{(i)}, P_{t|t}^{(i)}). \end{aligned}$$

To assess the reliability of the approximated posteriors with the particle methods, in this section, we establish a bound on how the approximation error in the parameter posterior affects the resulting state estimates. The following Proposition formalizes the result by relating the KL divergence between the true and approximate parameter posteriors to the total variation distance between the corresponding marginal state posteriors.

Proposition 2. *Let $\pi_t(\theta) = p(\theta_t | y_{1:t})$ denote the true parameter posterior and let $q_t(\theta)$ be its SGD/FSGD based particle approximation at time t . Let $p(x_t | y_{1:t})$ and $\tilde{p}(x_t | y_{1:t})$ denote the true and approximate marginal state posteriors, obtained by marginalizing the joint posterior $p(x_t, \theta_t | y_{1:t})$, over π_t and q_t , respectively. Then,*

$$\|p(x_t | y_{1:t}) - \tilde{p}(x_t | y_{1:t})\|_1 \leq \sqrt{2\text{KL}(q_t(\theta) \| \pi_t(\theta))}, \quad (27)$$

where $\|\cdot\|_1$ denotes the L^1 norm on the measurable space.

Proof. By definition we have,

$$\begin{aligned} p(x_t | y_{1:t}) &= \int p(x_t | \theta, y_{1:t}) \pi_t(\theta) d\theta, \\ \tilde{p}(x_t | y_{1:t}) &= \int p(x_t | \theta, y_{1:t}) q_t(\theta) d\theta, \end{aligned}$$

and the L^1 distance between the marginals is,

$$\begin{aligned} \|p(x_t | y_{1:t}) - \tilde{p}(x_t | y_{1:t})\|_1 &= \\ &= \int \left| \int p(x_t | \theta, y_{1:t}) [\pi_t(\theta) - q_t(\theta)] d\theta \right| dx_t. \end{aligned}$$

Applying the triangle inequality in the integral above yields,

$$\begin{aligned} \|p(x_t | y_{1:t}) - \tilde{p}(x_t | y_{1:t})\|_1 &\leq \\ &= \int \int |p(x_t | \theta, y_{1:t}) [\pi_t(\theta) - q_t(\theta)]| d\theta dx_t. \end{aligned} \quad (28)$$

The integrand on the right-hand side in (28) is nonnegative, thus we can exchange the order of integration:

$$\begin{aligned} &= \int \int |p(x_t | \theta, y_{1:t}) [\pi_t(\theta) - q_t(\theta)]| d\theta dx_t \\ &= \int \left(\int p(x_t | \theta, y_{1:t}) dx_t \right) |\pi_t(\theta) - q_t(\theta)| d\theta \\ &= \int |\pi_t(\theta) - q_t(\theta)| d\theta, \end{aligned} \quad (29)$$

as $p(x_t | \theta, y_{1:t})$ is a probability density in x_t for a fixed θ , it integrates to one. Combining (29) with (28) yields,

$$\|p(x_t | y_{1:t}) - \tilde{p}(x_t | y_{1:t})\|_1 \leq \|\pi_t(\theta) - q_t(\theta)\|_1. \quad (30)$$

Finally, Pinsker's inequality [26] relates the L^1 norm and the KL divergence as follows,

$$\|\pi_t(\theta) - q_t(\theta)\|_1 \leq \sqrt{2\text{KL}(q_t(\theta) \| \pi_t(\theta))}.$$

Combining the above inequality with (30), we obtain, $\|p(x_t | y_{1:t}) - \tilde{p}(x_t | y_{1:t})\|_1 \leq \sqrt{2\text{KL}(q_t(\theta) \| \pi_t(\theta))}$. \square

Proposition 2 provides a theoretical guarantee on the fidelity of the proposed SVGD-based parameter inference: if the divergence between the approximate and true parameter posteriors is small, then the corresponding marginal state estimate remains close in total variation.

Combining the error bound from Proposition 2 with Proposition 1 allows us to establish that sufficiently large number of SVGD iterations M , with sufficiently small step-sizes ϵ , monotonically tighten the upper bound on the total variation distance between the true and approximate marginal state posteriors. The following proposition formalizes this result.

Proposition 3. *Let $\pi_t(\theta) = p(\theta_t | y_{1:t})$ denote the true parameter posterior and let $\{q_{t,m}\}_{m \geq 0}$ be the sequence of proposal with SVGD iterates produced with a stepsize $0 < \epsilon \leq \epsilon_0$ as in Proposition 1 at time t . Let $p(x_t | y_{1:t})$ be the true marginal state posterior and let $\tilde{p}_m(x_t | y_{1:t})$ be the approximated marginal state posterior obtained by integrating w.r.t. $q_{t,m}$. Then at the population limit ($N \rightarrow \infty$), for all $m \geq 0$,*

$$\begin{aligned} \|p(x_t | y_{1:t}) - \tilde{p}_m(x_t | y_{1:t})\|_1 &\leq \sqrt{2\text{KL}(q_{t,m} \| \pi_t)} \\ &< \sqrt{2\text{KL}(q_{t,m-1} \| \pi_t)}. \end{aligned}$$

Thus, each SVGD update with $0 < \epsilon \leq \epsilon_0$ strictly reduces the upper bound on the L^1 error of the approximate state marginal unless $q_{t,m} = \pi_t$.

Proof. The proof straightforwardly follows from applying Proposition 1 to Proposition 2. \square

Proposition 3 shows that the refinement of the parameter posterior via SVGD directly improves the theoretical upper bound on the resulting state approximation error. Hence, under sufficiently small stepsizes, repeated SVGD updates jointly tighten the parameter and state posteriors in a monotone manner.

Remark 3. Although the practical SVGD implementation is based on a finite set of N particles, the theoretical analysis in Propositions 1–2, and Proposition 3, is carried out in asymptotically, assuming $N \rightarrow \infty$. In this regime, the particle system is interpreted as an empirical approximation to an underlying smooth density q_t , which evolves under the deterministic transport map $\theta \mapsto \theta + \epsilon\phi(\theta)$. This viewpoint is standard in SVGD theory (see, e.g., [16], [27]). The particle-based algorithm therefore serves as a finite-dimensional discretization of the mean-field SVGD dynamics analysed here.

VI. CASE STUDIES

In this section, we evaluate the performance of the proposed filtering algorithms on two case studies. The first one considers a nonlinear batch bioreactor process, highlighting the proposed filtering algorithm’s capability to handle time-varying nonlinearities and process uncertainties. In the second case study, we consider the problem of online training of a neural network to learn unknown dynamics of a nonlinear system.

A. Batch Bioreactor System

In this case study, we consider a nonlinear batch bioreactor model, commonly used to describe microbial fermentation processes. The reactor dynamics is governed by three state variables: biomass concentration X_t , substrate concentration S_t , and product concentration P_t . The continuous-time model of the system is obtained via mass balance equations (see [28]) and is described by:

$$\frac{dX_t}{dt} = \mu(S_t, \eta_t)X_t, \quad (31a)$$

$$\frac{dS_t}{dt} = -\frac{1}{Y_{xs}}\mu(S_t, \eta_t)X_t, \quad (31b)$$

$$\frac{dP_t}{dt} = Y_{px}\mu(S_t, \eta_t)X_t, \quad (31c)$$

where $\mu(S_t, \eta_t)$ denotes the specific growth rate, Y_{xs} is the yield coefficient of biomass on substrate, Y_{px} is the yield coefficient of product on biomass, and η_t is the mixing efficiency parameter.

The specific growth rate $\mu(S_t, \eta_t)$ follows the Haldane kinetics model, which accounts for substrate inhibition and dissolved oxygen effects:

$$\mu(S_t, \eta_t) = \mu_{\max} \frac{S_t}{K_s + S_t + \frac{S_t^2}{K_i}} \eta_t, \quad (32)$$

where μ_{\max} is the maximum growth rate, K_s and K_i are the half-saturation and inhibition constants, respectively.

The mixing efficiency parameter η_t is modeled as a stochastic, time-varying variable to capture gradual changes in reactor

TABLE I
MODEL AND SIMULATION PARAMETERS FOR THE BATCH BIOREACTOR SYSTEM.

Parameter	Symbol	Value
Maximum specific growth rate	μ_{\max}	0.4 h ⁻¹
Half-saturation constant	K_s	0.1
Inhibition constant	K_i	10.0
Yield coefficient (biomass/substrate)	Y_{xs}	0.5
Yield coefficient (product/biomass)	Y_{px}	0.6
Initial mixing efficiency	η_0	1.0
Final mixing efficiency	η_f	0.6
Sigmoid slope	α	0.05
Sigmoid shift	β	5.0
Process noise covariance	Q	$1 \times 10^{-6} I_3$
Measurement noise covariance	R	1×10^{-6}
Sampling period	t_s	0.2 h

performance, such as varying oxygen transfer or mixing conditions. Its evolution over time is described by,

$$\eta_t \sim \mathcal{N}(\mu_{\eta,t}, \sigma_{\eta}^2), \quad \mu_{\eta,t} = (1 - \sigma(\alpha t - \beta))\eta_0 + \sigma(\alpha t - \beta)\eta_f, \quad (33)$$

where $\sigma(\cdot)$ denotes the sigmoid function, η_0 and η_f define the initial and final expected efficiency values, and (α, β) control the transition rate and timing of the change, respectively. The model parameters and simulation settings used in this study are summarized in Table I.

The continuous-time model (31) is discretized using a fourth-order Runge–Kutta (RK4) method, and process and measurement noise terms are incorporated to yield the discrete-time state–space representation consistent with (1).

The objective of this case study is to jointly estimate the system states $x_t = [X_t \ S_t \ P_t]^\top \in \mathbb{R}^3$ and the time-varying mixing efficiency parameter $\theta_t = \eta_t \in \mathbb{R}$ from noisy measurements of the product concentration $y_t = P_t \in \mathbb{R}$. The performance of the proposed RBSGD and RBFSGD filters is benchmarked against an Extended Kalman Filter (EKF) and a Rao–Blackwellized Particle Filter (RBPF) (Algorithm 1). The RBSGD and RBFSGD filters employ $N = 5$ particles, each performing a single Fisher–Adam update ($M = 1$) per time step with a step size $\epsilon = 0.001$. For fair comparison, the RBPF is also implemented with 5 particles, and the parameter covariance Σ_θ is tuned empirically via trial and error. All of the filters considered are initialized with the same parameter estimates, state means and covariances.

The filters’ performances are assessed using the *Continuous Ranked Probability Score* (CRPS), which provides a scoring rule for evaluating the accuracy of probabilistic estimates. For a scalar measurement y and a predicted cumulative distribution function (CDF) F , the CRPS is defined as

$$\text{CRPS}(F, y) = \int_{-\infty}^{\infty} (F(z) - \mathbb{I}\{z \geq y\})^2 dz, \quad (34)$$

where $\mathbb{I}\{\cdot\}$ denotes the indicator function. Lower CRPS values indicate more accurate predictive distribution. The CRPS for Gaussian (EKF) and Gaussian–mixture (proposed filters) posterior predictive distributions can be computed using closed-form expressions.

Figure 1 compares the performance of the proposed RB-SGD, RBFSGD filters with the EKF and RBPF in estimating the reactor states X_t and S_t . The estimated product concentration P_t is not reported as it is considered as a measured state. The proposed filters demonstrate superior tracking performance in terms of CRPS, with tighter uncertainty bounds. Figure 2 illustrates the estimated mixing efficiency η_t , where the proposed methods accurately captures the time-varying transition while maintaining lower estimation variance compared to the RBPF.

To evaluate the impact of incorporating Fisher information into the proposed algorithm, a Monte Carlo study was performed using 50 independent realizations of the stochastic parameter η_t . Figure 3 illustrates the comparative performance of the RBFSGD, RBSGD, and RBPF filters in terms of CRPS. The results show that both SVGD-based methods outperform the RBPF baseline, achieving lower CRPS values. Furthermore, the Fisher-informed variant of the proposed filter (RBF-SGD) outperforms its non-informed counterpart (RBSGD), demonstrating the benefits of incorporating Fisher information for improved gradient scaling and uncertainty calibration. For fair comparison, identical hyperparameter settings were used for the RBFSGD and RBSGD filters.

B. Online training of neural networks

In the second case study, we consider a three-state nonlinear dynamical system governed by

$$\frac{dx_{t,1}}{dt} = x_{t,2}, \quad (35a)$$

$$\frac{dx_{t,2}}{dt} = x_{t,3}, \quad (35b)$$

$$\frac{dx_{t,3}}{dt} = -2x_{t,1} - 3x_{t,2} - 4x_{t,3} + u_t + f_{\text{nl}}(x_{t,1}, x_{t,2}, x_{t,3}), \quad (35c)$$

where the nonlinear term f_{nl} is defined as

$$f_{\text{nl}}(x_{t,1}, x_{t,2}, x_{t,3}) = x_{t,1}e^{x_{t,3}} + 0.2 \sin(x_{t,2}x_{t,3}) + x_{t,3} + x_{t,2}. \quad (35d)$$

Only the state $x_{t,1}$ is assumed to be measurable.

The equations (35) are discretized using RK4 scheme with sampling time $t_s = 0.01$, and additive process noise ($Q_t = 1 \times 10^{-4}I_3$) and measurement noise ($R_t = 0.1$) are included to account for model uncertainties and sensor noise.

The objective of this benchmark is to jointly estimate the system states $(x_{t,1}, x_{t,2}, x_{t,3})$, the measurement noise covariance R_t , and the parameters of a neural network that approximates the nonlinear mapping f_{nl} from the noisy observations of $x_{t,1}$. The neural network comprises two hidden layers with four neurons each, using hyperbolic tangent (*tanh*) activations, resulting in a total of 42 trainable parameters θ_t .

Online learning of the neural network parameters is achieved using the proposed RBFSGD filter. The parameter posterior is represented by $N = 10$ particles, each updated through $M = 15$ Fisher-Adam steps (Algorithm 3) at every time instance with the step size of $\epsilon = 2 \times 10^{-2}$. For comparison, an Extended Kalman Filter (EKF), in which f_{nl} is considered as a part of the process noise, is also implemented

as a baseline. All of the filters considered are initialized with the same parameter estimates.

Figure 4 depicts the state estimation results. The proposed RBFSGD filter exhibits better tracking accuracy (in terms of CRPS) compared to the EKF, as the nonlinear term f_{nl} is progressively learned by the RBFSGD filter from the measurement data.

Figure 5 presents the performance of the trained neural network, trained online by RBFSGD filter, in estimating $f_{\text{nl}}(x_{t,1}, x_{t,2}, x_{t,3})$ along with the filter performance in estimating the noise measurement covariance R_t . The filter is able to track the trend in the variation of f_{nl} and also to approximate the true value of the covariance R_t .

VII. CONCLUSION

This work introduced a Rao-Blackwellized filtering framework that integrates deterministic SVGD updates for online Bayesian parameter inference with Kalman-based state estimation. The resulting RBSGD and RBFSGD filters enable efficient joint state-parameter estimation in nonlinear, time-varying systems, without requiring manual tuning of proposal distributions. We established a theoretical bound linking the divergence between the true and approximate parameter posteriors to the total variation error in the marginal state distribution, providing a basic consistency guarantee for the proposed approximation. Two case studies demonstrated that the filters outperform classical EKF and RBPF benchmarks in terms of tracking accuracy and parameter identification, while yielding more expressive posterior representations.

Future research will investigate the integration of the estimated state-parameter distributions into probabilistic and robust control schemes.

APPENDIX

A. Proof of Proposition 1

The proof is based on the SVGD contraction argument from [16, Theorem 3.1, Lemma 3.2].

For brevity, in this proof, we drop the time index t and only consider the iteration index m . Recall that q_m is the distribution associated with updated parameters $\theta_m^{(i)}$ transported via $\theta_m^{(i)} = \theta_{m-1}^{(i)} + \epsilon \phi_{q_{m-1}, p}^*(\theta_{m-1}^{(i)})$. Thus, for a given set of parameters $\{\theta_{m-1}^{(i)}\}_{i=1}^N$, we can view q_m as a function of ϵ and let us denote it as $q_m(\epsilon)$. Consequently, we note that the proposal at the previous step is $q_{m-1} = q_m(0)$. A second-order Taylor expansion of the KL divergence under smoothness assumptions yields,

$$\begin{aligned} \text{KL}(q_m(\epsilon) \parallel \pi) &= \text{KL}(q_{m-1} \parallel \pi) + \epsilon \left. \frac{d}{d\epsilon} \text{KL}(q_m(\epsilon) \parallel \pi) \right|_{\epsilon=0} \\ &\quad + \frac{\epsilon^2}{2} \left. \frac{d^2}{d\epsilon^2} \text{KL}(q_m(\epsilon) \parallel \pi) \right|_{\epsilon=\xi}, \end{aligned} \quad (36)$$

for some $0 \leq \xi \leq \epsilon$.

Following [16, Lemma 3.2], at the population limit ($N \rightarrow \infty$), the first derivative equals

$$\left. \frac{d}{d\epsilon} \text{KL}(q_m(\epsilon) \parallel \pi) \right|_{\epsilon=0} = -\mathbb{D}(q_{m-1} \parallel \pi)^2, \quad (37)$$

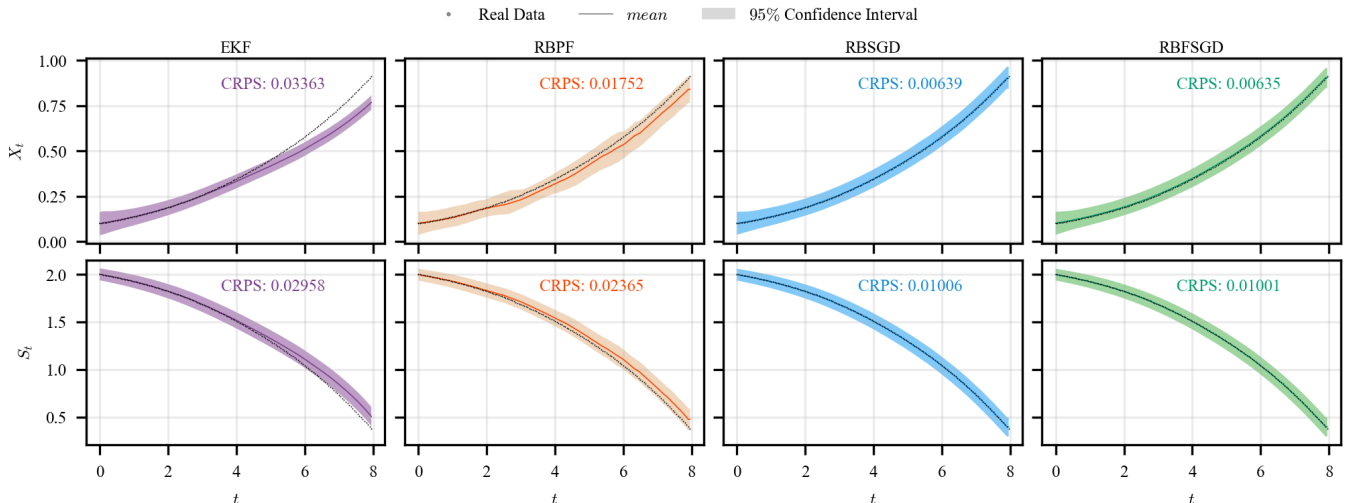


Fig. 1. State estimation performance: true states (dotted black), filter means (solid lines) and 95% confidence intervals (shaded areas). State X_t (top panels) and S_t (bottom panels).

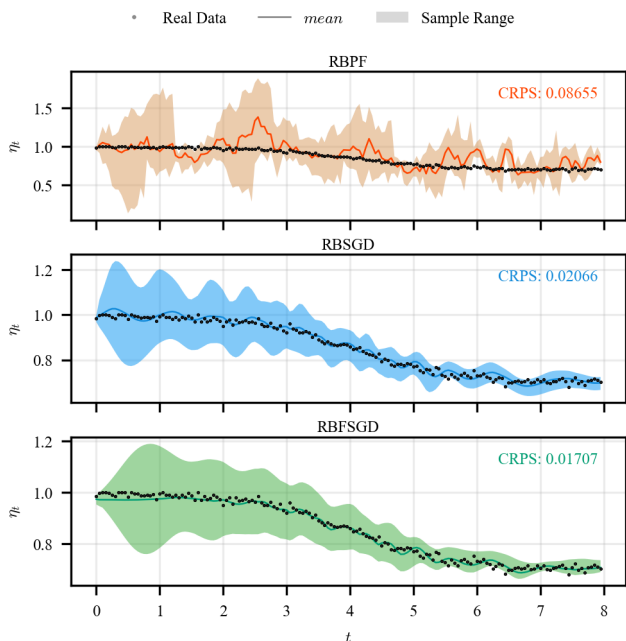


Fig. 2. Mixing efficiency estimation: true η_t (dotted black), filter means (solid lines) and uncertainty (shaded areas).

where $\mathbb{D}(q_{m-1}||\pi)^2$ is the Kernel Stein Discrepancy. Thus, when $q_{m-1} \neq \pi$, we can define $B_{m-1} > 0$ as the following:

$$B_{m-1} := \mathbb{D}(q_{m-1}||\pi)^2 \quad (38)$$

Boundedness of the Hessian of $\log \pi$ and smoothness of the kernel k ensure the second derivative in (36) is uniformly bounded by a constant $C < \infty$. Thus via (36), (37), and (38), we have

$$\text{KL}(q_m(\epsilon)||\pi) \leq \text{KL}(q_{m-1}||\pi) - \epsilon B_{m-1} + \frac{\epsilon^2}{2} C, \quad (39)$$

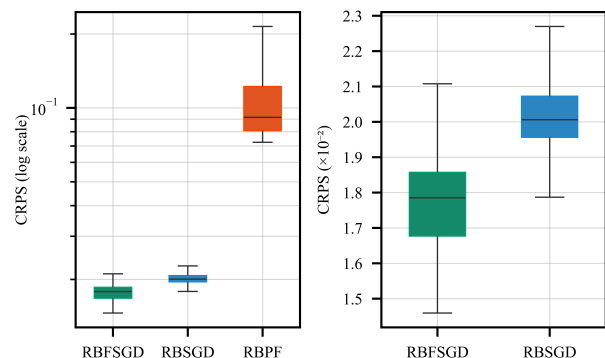


Fig. 3. Filter performance on the Monte Carlo study: The left panel shows the log-scaled CRPS comparison for the RBFSGD filter, RBSGD filter, and RBPF across 50 independent realizations of η_t . The right panel shows the zoomed-in boxplot from the left panel for RBFSGD and RBSGD.

Finally, by choosing $\epsilon < \epsilon_0 = \frac{2B_{m-1}}{C}$, we obtain (15). This completes the proof.

REFERENCES

- [1] Y. Huang, Y. Zhang, Z. Wu, N. Li, and J. Chambers, "A novel adaptive Kalman filter with inaccurate process and measurement noise covariance matrices," *IEEE Transactions on Automatic Control*, vol. 63, no. 2, pp. 594–601, 2017.
- [2] S. Särkkä and L. Svensson, *Bayesian filtering and smoothing*, vol. 17. Cambridge University Press, 2023.
- [3] R. Van Der Merwe and E. A. Wan, "The square-root unscented Kalman filter for state and parameter-estimation," in *2001 IEEE International Conference on Acoustics, Speech, and Signal Processing.*, vol. 6, pp. 3461–3464, IEEE, 2001.
- [4] Q. Ge, T. Shao, Z. Duan, and C. Wen, "Performance analysis of the Kalman filter with mismatched noise covariances," *IEEE Transactions on Automatic Control*, vol. 61, no. 12, pp. 4014–4019, 2016.
- [5] B. J. Odelson, M. R. Rajamani, and J. B. Rawlings, "A new autocovariance least-squares method for estimating noise covariances," *Automatica*, vol. 42, no. 2, pp. 303–308, 2006.
- [6] M. Karasalo and X. Hu, "An optimization approach to adaptive Kalman filtering," *Automatica*, vol. 47, no. 8, pp. 1785–1793, 2011.

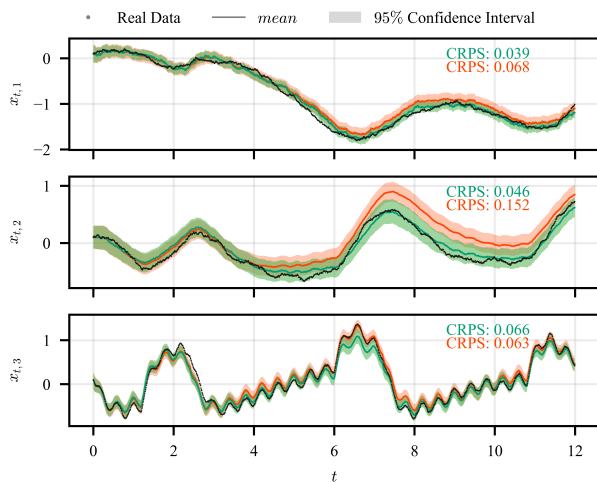


Fig. 4. State estimation performance: true states (dotted black), RBFSGD filter mean (solid green) and uncertainty (shaded green), EKF mean (solid orange) and uncertainty (shaded orange).

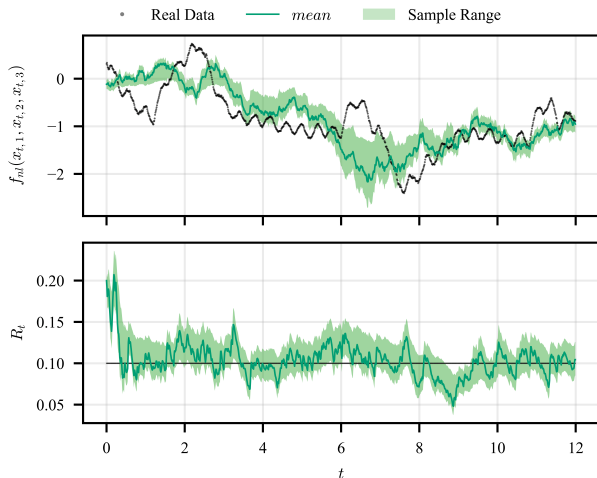


Fig. 5. Parameter estimation performance for the nonlinear system: true parameter (dotted black), RBFSGD filter mean estimate (solid green), estimated uncertainty (shaded green)

[7] Q. Ge, Y. Li, Y. Wang, X. Hu, H. Li, and C. Sun, “Adaptive Kalman filtering based on model parameter ratios,” *IEEE Transactions on Automatic Control*, vol. 69, no. 9, pp. 6230–6237, 2024.

[8] A. Bemporad, “Recurrent Neural Network Training with Convex Loss and Regularization Functions by Extended Kalman Filtering,” *IEEE Transactions on Automatic Control*, vol. 67, no. 12, pp. 6330–6345, 2022.

[9] E. Archer, I. M. Park, L. Buesing, J. Cunningham, and L. Paninski, “Black box variational inference for state space models,” *arXiv preprint arXiv:1511.07367*, 2015.

[10] S. S. J. Hartikainen, “Variational Bayesian adaptation of noise covariances in non-linear Kalman filtering,” *arXiv preprint arXiv:1302.0681*, 2013.

[11] M. S. Arulampalam, S. Maskell, N. Gordon, and T. Clapp, “A tutorial on particle filters for online nonlinear/non-Gaussian Bayesian tracking,” *IEEE Transactions on Signal Processing*, vol. 50, no. 2, pp. 174–188, 2002.

[12] K. Murphy and S. Russell, “Rao-Blackwellised particle filtering for dynamic Bayesian networks,” in *Sequential Monte Carlo methods in practice*, pp. 499–515, Springer, 2001.

[13] M. Mejari and D. Piga, “Maximum-A-Posteriori Estimation of Linear

Time-Invariant State-Space Models via Efficient Monte-Carlo Sampling,” *ASME Letters in Dynamic Systems and Control*, vol. 2, no. 1, 2022.

[14] T. Schon, F. Gustafsson, and P.-J. Nordlund, “Marginalized particle filters for mixed linear/nonlinear state-space models,” *IEEE Transactions on Signal Processing*, vol. 53, no. 7, pp. 2279–2289, 2005.

[15] T. Badar, S. Särkkä, Z. Zhao, and A. Visala, “Rao-Blackwellized particle filter using noise adaptive Kalman filter for fully mixing state-space models,” *IEEE Transactions on Aerospace and Electronic Systems*, vol. 60, no. 5, pp. 6972–6982, 2024.

[16] Q. Liu and D. Wang, “Stein variational gradient descent: A general purpose bayesian inference algorithm,” *Advances in Neural Information Processing Systems*, vol. 29, 2016.

[17] C. Liu and J. Zhu, “Riemannian Stein variational gradient descent for Bayesian inference,” in *Proceedings of the AAAI Conference on Artificial Intelligence*, vol. 32, 2018.

[18] G. Detommaso, T. Cui, Y. Marzouk, A. Spantini, and R. Scheichl, “A Stein variational Newton method,” *Advances in Neural Information Processing Systems*, vol. 31, 2018.

[19] F. A. Maken, F. Ramos, and L. Ott, “Stein particle filter for nonlinear, non-Gaussian state estimation,” *IEEE Robotics and Automation Letters*, vol. 7, no. 2, pp. 5421–5428, 2022.

[20] S.-I. Amari, “Natural gradient works efficiently in learning,” *Neural Computation*, vol. 10, no. 2, pp. 251–276, 1998.

[21] D. Hwang, “FAdam: Adam is a natural gradient optimizer using diagonal empirical Fisher information,” *arXiv preprint arXiv:2405.12807*, 2024.

[22] D. M. Gomes, Y. Zhang, E. Belilovsky, G. Wolf, and M. S. Hosseini, “AdaFisher: Adaptive Second Order Optimization via Fisher Information,” in *13th International Conference on Learning Representations*, 2025.

[23] N. N. Schraudolph, “Fast curvature matrix-vector products for second-order gradient descent,” *Neural Computation*, vol. 14, no. 7, pp. 1723–1738, 2002.

[24] J. Martens, “Deep learning via Hessian-free optimization,” in *Proceedings of the 27th International Conference on International Conference on Machine Learning, ICML’10, (Madison, WI, USA)*, p. 735–742, Omnipress, 2010.

[25] O. Vinyals and D. Povey, “Krylov subspace descent for deep learning,” in *Artificial Intelligence and Statistics*, pp. 1261–1268, PMLR, 2012.

[26] M. S. Pinsker, “Information and information stability of random variables and processes,” *Holden-Day*, 1964.

[27] A. Korba, P.-C. Aubin-Frankowski, S. Majewski, and P. Ablin, “Kernel Stein discrepancy descent,” in *International Conference on Machine Learning*, pp. 5719–5730, PMLR, 2021.

[28] N. Marcos, M. Guay, D. Dochain, and T. Zhang, “Adaptive extremum-seeking control of a continuous stirred tank bioreactor with Haldane’s Kinetics,” *Journal of Process Control*, vol. 14, no. 3, pp. 317–328, 2004.